Journal of Nuclear Medicine, published on July 21, 2014 as doi:10.2967/jnumed.114.141218

Preparation and Preliminary Evaluation of ^{63}Zn-Zinc Citrate as a Novel PET Imaging Biomarker for Zinc

Timothy R. DeGrado[1], Mukesh K. Pandey[1], John F. Byrne[2], Hendrik P. Engelbrecht[1], Huailei Jiang[1], Alan B. Packard[3], Kevin A. Thomas[1], Mark S. Jacobson[1], Geoffrey L. Curran[1], and Val J. Lowe[1]

[1]Department of Radiology, Mayo Clinic, Rochester, Minnesota; [2]Brigham and Women's Hospital, Harvard Medical School, Boston, Massachusetts; and [3]Boston Children's Hospital, Harvard Medical School, Boston, Massachusetts

Abnormalities of zinc homeostasis are indicated in many human diseases. A noninvasive imaging method for monitoring zinc in the body would be useful to understand zinc dynamics in health and disease. To provide a PET imaging agent for zinc, we have investigated production of ^{63}Zn (half-life, 38.5 min) via the ^{63}Cu(*p,n*)^{63}Zn reaction using isotopically enriched solutions of ^{63}Cu-copper nitrate. A solution target was used for rapid isolation of the ^{63}Zn radioisotope from the parent ^{63}Cu ions. Initial biologic evaluation was performed by biodistribution and PET imaging in normal mice. **Methods:** To produce ^{63}Zn, solutions of ^{63}Cu-copper nitrate in dilute nitric acid were irradiated by 14-MeV protons in a low-energy cyclotron. An automated module was used to purify ^{63}Zn from ^{63}Cu in the target solution. The ^{63}Cu–^{63}Zn mixture was trapped on a cation-exchange resin and rinsed with water, and the ^{63}Zn was eluted using 0.05 N HCl in 90% acetone. The resulting solution was neutralized with $NaHCO_3$, and the ^{63}Zn was then trapped on a carboxymethyl cartridge, washed with water, and eluted with isotonic 4% sodium citrate. Standard quality control tests were performed on the product according to current good manufacturing practice, including radionuclidic identity and purity, and measurement of nonradioactive Zn^{+2}, Cu^{+2}, Fe^{+3}, and Ni^{+2} by ion-chromatography high-performance liquid chromatography. Biodistribution and PET imaging studies were performed in B6.SJL mice after intravenous administration of ^{63}Zn-zinc citrate. ^{63}Cu target material was recycled by eluting the initial resin with 4N HNO_3. **Results:** Yields of 1.07 ± 0.22 GBq (uncorrected at 30–36 min after end of bombardment) of ^{63}Zn-zinc citrate were obtained with a 1.23 M ^{63}Cu-copper nitrate solution. Radionuclidic purity was greater than 99.9%, with copper content lower than 3 μg/batch. Specific activities were 41.2 ± 18.1 MBq/μg (uncorrected) for the ^{63}Zn product. PET and biodistribution studies in mice at 60 min showed expected high uptake in the pancreas (standard uptake value, 8.8 ± 3.2), liver (6.0 ± 1.9), upper intestine (4.7 ± 2.1), and kidney (4.2 ± 1.3). **Conclusion:** A practical and current good manufacturing practice–compliant preparation of radionuclidically pure ^{63}Zn-zinc citrate has been developed that will enable PET imaging studies in animal and human studies. ^{63}Zn-zinc citrate showed the expected biodistribution in mice.

Key Words: ^{63}Zn; PET; radioisotope production; solution target

J Nucl Med 2014; 55:1–7
DOI: 10.2967/jnumed.114.141218

Zinc is an essential metal in the body that is at the reactive center of more than 300 metabolic enzymes and has fundamental roles in protein structure and protein–protein interactions (*1*). It participates in the tertiary, quaternary, and quinary structure of proteins; in protein aggregation; and in the structure of protein domains for interactions with other proteins, DNA/RNA, and lipids. Zinc deficiency affects about 2 billion people in the developing world (*2*), whereas excess zinc consumption can also cause detrimental effects of ataxia, lethargy, and copper deficiency. Disruption of zinc homeostasis may be involved in metabolic syndrome, diabetes, and diabetic complications (*3*). Zinc homeostasis may play an important role in certain cancer types, including pancreatic cancer (*4*), prostate cancer (*5*), and breast cancer (*6*). Also, zinc is associated with the aggregation of β-amyloid proteins that accumulate in the brains of patients with Alzheimer disease (AD) (*7*). Metal chelation therapy is under investigation for treatment of AD with the intent of altering zinc and copper binding within β-amyloid deposits in the brain (*8*). Clearly, a noninvasive method to measure zinc dynamics in the body would be of high interest for understanding the pathophysiology of a broad range of diseases. It may also be useful for monitoring therapies that are directed at changing zinc homeostasis.

There are 3 positron-emitting isotopes of zinc that have potential to be used as PET biomarkers of zinc kinetics in living systems: ^{62}Zn, ^{63}Zn, and ^{65}Zn (Table 1). ^{62}Zn (half-life [$T_{1/2}$], 9.26 h) is compromised for imaging of zinc biodistribution because its daughter isotope ^{62}Cu is also a positron emitter that may confound the interpretation of the PET images. Nevertheless, ^{62}Zn has been effectively used preclinically as a zinc biomarker of pancreatic exocrine function (*9*). ^{65}Zn is impractical for clinical imaging because of its 244-d $T_{1/2}$ but has served as a zinc biomarker in central nervous system investigations (*10*). The potential of ^{63}Zn as a PET imaging tracer is supported by its attractive physical decay characteristics ($T_{1/2}$, 38.5 m; mean β^+ energy, 0.99 MeV; total β^+ intensity, 93%) and the feasibility of cyclotron production via the ^{63}Cu(*p,n*)^{63}Zn reaction in low-energy proton accelerators (*11,12*). Although the shorter $T_{1/2}$ of ^{63}Zn may limit its ability to assess longer biologic turnover times, it is sufficient to monitor initial transport of zinc from the blood to tissues and further transport processes that have turnover times in the order of 2 h or less. For example, ^{63}Zn should be well suited to study transport kinetics of zinc into the pancreas or prostate or across the blood–brain barrier.

[Table 1]

^{63}Zn has been produced by irradiating natural copper foils with protons through the ^{nat}Cu(*p,n*)^{63}Zn nuclear reaction that exhibits high cross section values at low proton energies (*11,12*). Because

Received Apr. 8, 2014; revision accepted May 30, 2014.
For correspondence or reprints contact: Timothy R. DeGrado, Molecular Imaging Research, Mayo Clinic, 200 First St. SW, Rochester, MN 55905.
E-mail: degrado.timothy@mayo.edu
Published online Jul. 21, 2014.

TABLE 1
Positron-Emitting Isotopes of Zinc

Parent nucleus	Decay mode*	Daughter nucleus	$T_{1/2}$	Mean β^+ energy (MeV)	Total β^+ intensity	High-energy emissions (MeV)†
^{62}Zn	EC, β^+	^{62}Cu ($T_{1/2}$, 9.7 m)	9.26 h	0.259	8.4	0.508 (15%), 0.55 (15%), 0.60 (26%)
^{63}Zn	EC, β^+	^{63}Cu (stable)	38.47 m	0.992	92.7	0.67 (8%), 0.96 (7%)
^{65}Zn	EC, β^+	^{65}Cu (stable)	243.9 d	0.1425	1.42	1.11 (50.6%)

*Electron capture.
†Data in parentheses are intensity percentages.

natural copper is composed of 69.2% ^{63}Cu and 31.8% ^{65}Cu, small fractions of ^{65}Zn were produced via the ^{65}Cu(p,n)^{65}Zn reaction, which would preclude applications in clinical imaging. In the present study, we investigate the feasibility to produce pure ^{63}Zn using isotopically enriched ^{63}Cu as parent material. On the basis of our recent findings on solution targets (*13*), we now report use of a solution target filled with ^{63}Cu-copper nitrate in dilute nitric acid to produce ^{63}Zn. A methodology for rapid separation of the ^{63}Zn product from ^{63}Cu was also developed. Although lower quantities of ^{63}Zn can be produced in a solution target relative to a solid target, isotopically enriched ^{63}Cu foils are not commercially available, and the solution target approach avoids the need to dissolve the target after irradiation, thus saving time in the purification process. The purification process was automated using a radiochemistry module built in-house. Finally, the ^{63}Zn-zinc citrate product was preliminarily evaluated for uptake characteristics by biodistribution in normal B6.SJL mice.

MATERIALS AND METHODS

The AG 50W-X8 (H^+ form, 200–400 mesh) resin (Bio-Rad) was used as received and slurry-packed with water into a glass Econo-Column (Bio-Rad). The water (18 mΩ) was purified in-house (Barnstead Nanopure system by Thermo Scientific). The HCl and HNO_3 were obtained as trace metal grade from Fisher Scientific. Isotopically enriched ^{63}Cu metal (99.9% enrichment) was obtained from Cambridge Isotope Laboratories. Acetone and $NaHCO_3$ were obtained from Sigma-Aldrich. Sterile 4% sodium citrate solution, U.S. Pharmacopeia (USP), was obtained from Fenwal Inc. Sep-Pak CM Light cartridges (Waters Corp.) were prerinsed with 5 mL of water. The radioactivity readings were recorded using a CRC dose calibrator (#480 setting, CRC-55tPET; Capintec).

Production and Purification of ^{63}Zn

A PETtrace cyclotron (GE Healthcare) was used. The solution target was developed in-house as previously described (*14*). Briefly, it consisted of a 1.6-mL water-cooled tantalum target insert that was separated from the cyclotron by dual foils (aluminum and Havar [Goodfellow]) with a helium cooling channel in between. Incident proton energy was degraded from 16.4 to approximately 14 MeV at the target solution. The isotopically enriched ^{63}Cu powder (99.9% enriched, 1.0 g, 15.9 mmol) was dissolved in excess HNO_3 and then evaporated to dryness under vacuum to form $^{63}Cu(NO_3)_2 \cdot xH_2O$. By weighing the dried material (3.8 g), we estimated that the ratio of water molecules to copper nitrate was approximately 3. To prepare a 1.7 M $^{63}Cu(NO_3)_2$ target solution, 0.74 g of $^{63}Cu(NO_3)_2 \cdot xH_2O$ and 12 μL of concentrated nitric acid were added to sufficient water to bring the total volume to 1.8 mL. The concentration of HNO_3 (~0.1N) was sufficient to prevent in-target precipitation of copper hydroxide while reducing water radiolysis (*13*).

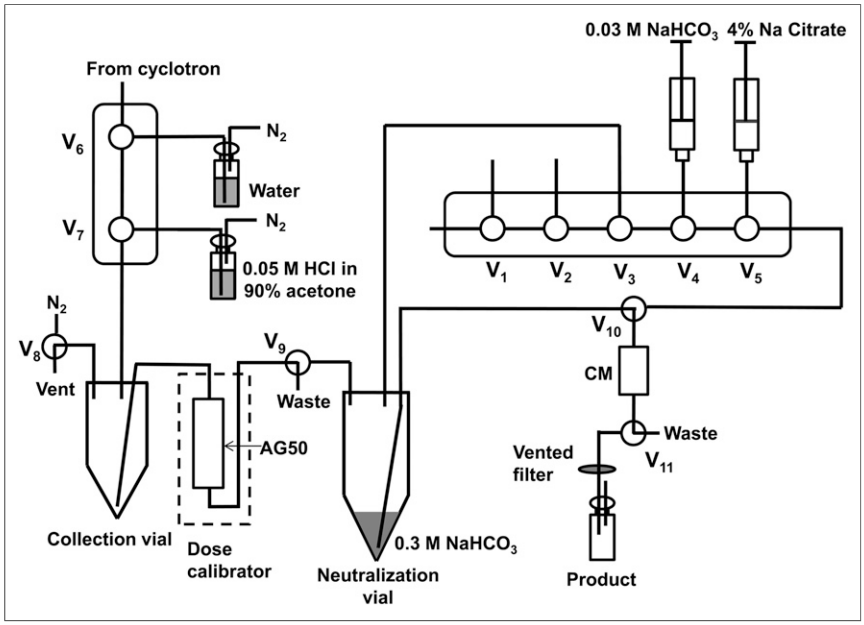

FIGURE 1. Schematic of automated module for preparation of ^{63}Zn-zinc citrate. Valves V1–V5 are composed of a disposable cassette that is mounted to front of module. All other valves are nondisposable Teflon (DuPont) solenoid valves.

The $Cu(NO_3)_2 \cdot xH_2O$ solution (1.8 mL) was loaded into the cyclotron target using an automated valve system (*13,14*). The target was pressurized with air (40–45 psi) and irradiated at 20 μA for 60 min. Pressure rose in the target until reaching a plateau of 110–130 psi at approximately 20 min after the start of irradiation. After irradiation, the target material was delivered to an in-house–developed automated radiosynthesis module (Fig. 1) for further processing. The target material was first delivered into a collection vial in the hot cell. The target was rinsed with water (1.8 mL) that was delivered to the same collection vial to yield a final volume of approximately 3.6 mL. Both ^{63}Zn and ^{63}Cu were trapped on a column of AG 50W-X8 resin (6 g), which was prewashed with 4N HNO_3 (5 mL) and then flushed with water (75 mL) before each production and placed in a dose calibrator for measurement of [**Fig. 1**]

jnm141218-pm ■ 7/18/14

trapped radioactivity. The ^{63}Zn solution was loaded onto the AG 50W-X8 column at a flow rate of approximately 2 mL/min. The column was washed with 9 mL of water to remove ^{13}N and ^{11}C byproducts that were formed during the irradiation. Following the work of Guerra-Gómez et al. (*12*), the ^{63}Zn was eluted with 0.05 N HCl in 90% acetone (30 mL) and transferred to a 100-mL neutralization flask that was prefilled with 8 mL of a 0.3 M $NaHCO_3$ solution. After brief stirring, the resulting mixture was passed through a carboxymethyl cartridge (CM Sep-Pak Light; Waters) under 20 psi driving pressure. The carboxymethyl cartridge was washed with 0.03 M $NaHCO_3$ (10 mL) to remove the acetone without loss of ^{63}Zn. Finally, the product was eluted from the carboxymethyl cartridge with 2–5 mL of 4% sodium citrate USP solution, passed through a 0.2-μm sterilizing filter, and collected in a sterile empty vial. In initial runs, referred to as non-cGMP (current good manufacturing practice), metal needles were avoided, but in final runs performed according to cGMP, disposable metal needles were used in the process of sterile filtration, procurement of the quality control (QC) sample, and dilution of the product (2 mL) with sterile saline (8 mL).

The $^{63}Cu(NO_3)_2$ was recycled by washing the AG 50W-X8 column in retrograde direction with water (20 mL), followed by elution (again retrograde) of the ^{63}Cu with 4N HNO_3 (~20 mL). The column was further washed with water (75 mL) to remove any residual acid. In initial runs, the AG column was reused. For the final runs that were performed according to cGMP, the AG column was prepared fresh before each run. The recovered $^{63}Cu(NO_3)_2$ solution was dried under vacuum and the residual $^{63}Cu(NO_3)_2 \cdot xH_2O$ reconstituted in 0.1 M HNO_3 as described above.

QC of ^{63}Zn-Zinc Citrate Product

The ^{63}Zn-zinc citrate product was submitted for standard QC analyses for radiopharmaceutical preparation, including optical clarity by appearance, pH, radionuclidic identity (half-life and high-purity germanium γ spectroscopy, DSA-1000; Canberra), radionuclidic purity (high-purity germanium spectroscopy), residual solvents (GC-FID; SRI Instruments), filter integrity, pyrogens (endotoxin test), and sterility. For radiochemical and chemical purity, the QC samples were analyzed using a high-performance liquid chromatography (HPLC) system (Dionex ICS-5000; ThermoFisher), equipped with an IonPac CS5A analytic column (4 × 250 mm; Dionex, ThermoFisher) and PC10 postcolumn pneumatic delivery system (Dionex, ThermoFisher) to mix the dye 4-(2-pyridylazo)resorcinol (PAR) (Dionex, ThermoFisher) for spectrophotometric detection at 530 nm of Zn^{+2}, Cu^{+2}, Fe^{+3}, and Ni^{+2}. The flow rate of the mobile phase (MetPac Eluent; Dionex, ThermoFisher) was 1.2 mL/min. The flow rate of PAR diluent was 0.6 mL/min. The HPLC also had in-line radioactivity detection (Carroll and Ramsey). Because the radioactivity detector was placed before the postcolumn PAR dilution manifold, there was an approximate 0.3-min delay between the radioactivity and ultraviolet data recording.

Biodistribution and PET Imaging of ^{63}Zn-Zinc Citrate in Mice

Biodistribution characteristics of ^{63}Zn-zinc citrate were investigated in male B6.SJL mice ($n = 4$) (Jackson Laboratories) under the approval of the Mayo Clinic Institutional Animal Care and Use Committee. Animals were administered ^{63}Zn-zinc citrate (~1.8–3.6 MBq) into a tail vein and euthanized at 60 min for biodistribution analysis. Tissues were weighed and counted for radioactivity. Biodistribution data were expressed as standardized uptake value (SUV) = (counts/g)tissue/(injected dose counts/weight of mouse (g)). In 1 mouse, dynamic small-animal PET (Inveon; Siemens) images were acquired after intravenous injection of 14.8 MBq of ^{63}Zn-zinc citrate. The mouse was anesthetized using 1.5% isoflurane gas. Images were reconstructed using an ordered-subset expectation maximization iterative algorithm. Image resolution was compared for ^{63}Zn and ^{18}F by imaging a microresolution phantom filled at a radioactivity concentration similar for the 2 PET radionuclides (~3.7 MBq/mL).

Statistics

Biodistribution data were expressed as mean ± SD. Statistical comparison of analytic data between groups of runs was performed using the 2-tailed Student *t* test. Statistical comparison of intracerebral regional uptake of ^{63}Zn was performed using ANOVA. *P* values of less than 0.05 were considered statistically significant.

TABLE 2
Production Yield, Specific Activity, and Metal Impurities in ^{63}Zn-Zinc Citrate Preparations

Group	^{63}Cu used (mg/batch)	Concentration of $^{63}Cu(NO_3)_2$ (M)	Batch yield after process* (GBq)	Saturated yield after process* (MBq/μA)	Specific activity† (MBq/μg)	Metals (μg)
Non-cGMP‡	321 ($n = 3$)	1.7	3.06 ± 0.16	309 ± 17	108 ± 62 (range, 36–144)	Fe^{+3}: 13.0 ± 2.1
						Cu^{+2}: 40.5 ± 16.1
						Ni^{+2}: ND
						Zn^{+2}: 16.1 ± 8.3
cGMP§	232 ($n = 6$)	1.23	2.00 ± 0.39	151 ± 29	41.2 ± 18.1 (range, 19.2–66.5)	Fe^{+3}: 28.2 ± 1.7‖
						Cu^{+2}: 2.7 ± 1.8‖
						Ni^{+2}: ND
						Zn^{+2}: 29.5 ± 9.4

*Decay-corrected to end of bombardment, processing time was 30–36 min.
†At end of synthesis.
‡Non-cGMP process, reused AG50W-X8 resin.
§cGMP process, new AG50W-X8 resin.
‖$P < 0.05$ versus non-cGMP processing.
All irradiations were at beam current of 20 μA for 60 min.
ND = not detected.

jnm141218-pm ■ 7/18/14

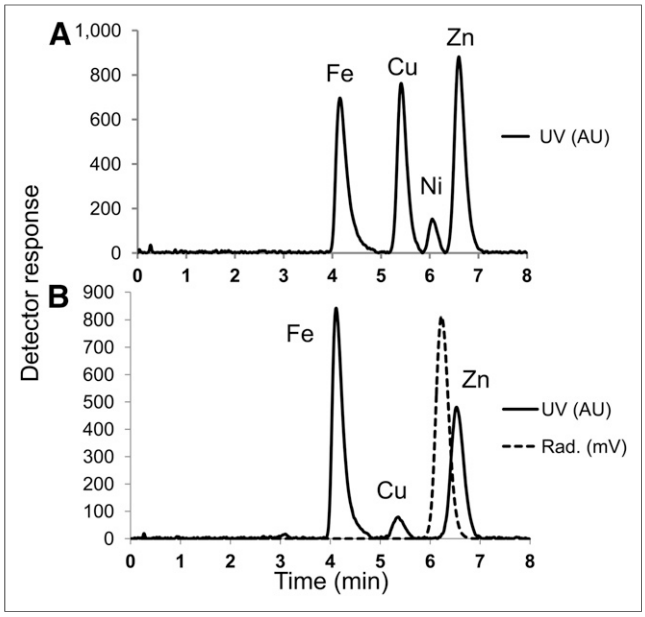

FIGURE 2. Radio–high-performance liquid chromatograms of cGMP ^{63}Zn-zinc citrate product. (A) UV chromatogram (530 nm) for reference standards for 2.5 mg/L each of Fe^{+3}, Cu^{+2}, Ni^{+2}, and Zn^{+2}. (B) UV and radio–high-performance liquid chromatograms for representative cGMP run of ^{63}Zn-zinc citrate product. There is 0.3-min delay between UV detector and radioactivity detector. Rad. = radio; UV = ultraviolet.

RESULTS

Production and Isolation of ^{63}Zn

Proton irradiations of $^{63}Cu(NO_3)_2$ solutions (1.7 or 1.23 M) were performed for 60 min at 20 μA (Table 2). After the target rinse dilution to approximately 0.05 M HNO_3, both the ^{63}Cu and the ^{63}Zn were trapped on the AG 50W-X8 cation-exchange resin (Fig. 1). A further 9 mL of water rinse removed a large fraction of the ^{13}N, ^{11}C, and ^{18}F contaminants generated during the irradiation. ^{63}Zn was eluted from the AG column by washing with 30 mL of 0.05 M HCl in 90% acetone. The elution of ^{63}Zn from the AG column was followed by monitoring the amount of radioactivity in the dose calibrator. The ^{63}Zn was further processed by neutralization with $NaHCO_3$, trapping on a carboxymethyl cartridge, rinsing with 10 mL of a 0.03 M $NaHCO_3$ solution, elution with 2–5 mL of 4% sodium citrate USP solution through a 0.2-μm sterilizing filter, and collection in a sterile empty vial. The time of processing was 30–36 min. Calculated saturated yields (corrected) of processed ^{63}Zn-zinc citrate were 309 ± 17 and 151 ± 29 MBq/μA, respectively, for 1.7 and 1.23 M $^{63}Cu(NO_3)_2$ solutions (Table 2). An uncorrected yield (at the end of processing) of 1.53 ± 0.10 GBq of ^{63}Zn-zinc citrate was obtained from 60-min irradiations of a 1.7N $^{63}Cu(NO_3)_2$ solution (n = 3). This yield was similar to the approximate 1.4-GBq yield reported by Guerra-Gómez et al. by irradiation and processing of solid natural copper foil (*12*). $^{63}Cu(NO_3)_2$ was successfully recovered (>85% recovery) and reirradiated several times with no degradation of radionuclidic purity of ^{63}Zn product.

[Table 2]

QC Tests

All standard radiopharmaceutical QC tests were passed, including appearance, half-life (38.5 ± 0.1 min), pH (6.5), endotoxins, and sterility. Representative radio–high-performance liquid chromatograms are shown in Figure 2. A single radioactive peak at 6.3 min corresponded to the nonradioactive Zn^{+2} retention time of 6.6 min, consistent with the time delay of 0.3 min between the radioactivity detector and the following ultraviolet detector. The analysis of metal ions in the product showed significant levels (2.6–40.5 μg/batch) of nonradioactive Zn^{+2}, Cu^{+2}, and Fe^{+3}. Ni^{+2}, however, was not detected in QC samples at a minimum detection level of approximately 1 μg/mL. Copper levels were low but significantly higher in the non-cGMP product than in the cGMP product (40 ± 16 vs. 2.7 ± 1.8 μg) likely because the non-cGMP product was prepared using recycled AG resin that had retained small quantities of raw material ^{63}Cu that were subsequently released in later runs. In contrast, the iron levels were higher in the cGMP runs relative to the non-cGMP runs (28.2 ± 1.7 vs. 13.0 ± 2.1). The greater use of disposable stainless steel needles during cGMP processing is likely responsible for the higher levels of iron in the cGMP runs. Radionuclide purity was found to be greater than 99.9% by high-purity germanium γ spectrometry after the end of synthesis, with the known major emissions at 511 keV (185.5%), 670 keV (8.2%), and 962 keV (6.5%) (Fig. 3A). There were no detectable γ emissions above background remaining in the samples 24 h after synthesis (Fig. 3B). Specific activities of 41.2 ± 18.1 MBq/μg (uncorrected) for the ^{63}Zn product were obtained. Thus, for a 370-MBq dose for a human study, approximately 9 μg (0.14 μmol) zinc would be administered. This level of zinc would represent a negligible amount, compared with the plasma levels of zinc of approximately 10 μM (*10*).

[Fig. 3]

Biodistribution and PET Imaging in Normal Mice

The biodistribution at 1 h showed the pancreas to have the highest SUV of 8.8 ± 3.2, with high uptake also seen in the liver, kidney, and upper intestine (Table 3). Intestinal uptake likely reflected secretion of radioactivity by the pancreas. The whole-brain SUV was 0.24 ± 0.09, showing moderate retention in the brain. The intracerebral regions did not show statistically significant differences in SUVs. Thus, brain uptake of ^{63}Zn was similar over the

[Table 3]

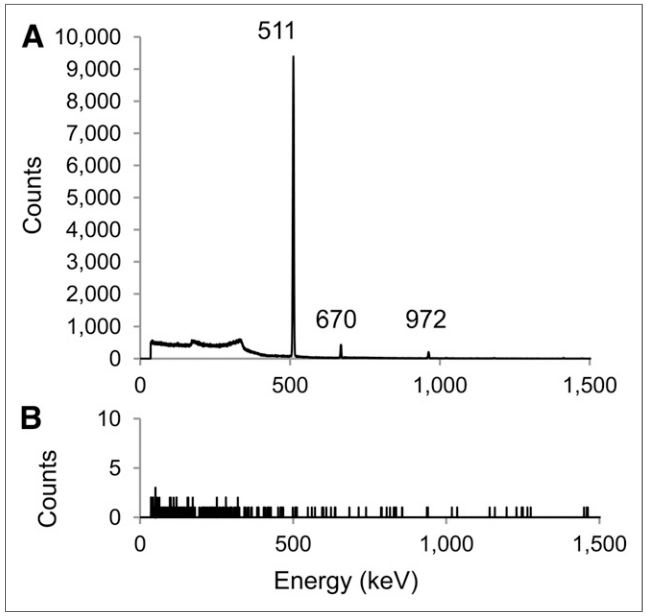

FIGURE 3. High-purity germanium detector γ spectrometry of ^{63}Zn-zinc citrate product at 90 min (A) after end of synthesis and 24 h (B) after end of synthesis.

TABLE 3
Biodistribution of ^{63}Zn-Zinc Citrate in Normal B6.SJL Mice (n = 4) at 1 Hour After Intravenous Administration

Tissue	SUV
Blood	0.57 ± 0.25
Heart	1.12 ± 0.23
Lung	2.06 ± 0.62
Liver	5.97 ± 1.92
Pancreas	8.78 ± 3.22
Kidney	4.21 ± 1.30
Upper intestine	4.72 ± 2.18
Muscle	0.21 ± 0.08
Bone	0.76 ± 0.34
Spleen	2.30 ± 1.01
Prostate	0.58 ± 0.23
Seminal vesicles	1.69 ± 0.79
Whole brain	0.24 ± 0.09
Cortex	0.19 ± 0.07
Caudate nuclei	0.37 ± 0.23
Hippocampus	0.48 ± 0.37
Thalamus	0.26 ± 0.10
Brain stem	0.25 ± 0.09
Cerebellum	0.31 ± 0.14

regions studied. The small-animal PET images were consistent with the biodistribution (Fig. 4A), showing high uptake in abdominal tissues (liver and gastrointestinal tract). [Fig. 4]

Microresolution Phantom Study

PET images of the microresolution phantom showed that capillary tubes filled with ^{63}Zn solution could not be resolved for tube separations up to 3 mm, whereas ^{18}F allowed for visualization of tube separations in the range of 2.0–2.5 mm (Fig. 4B).

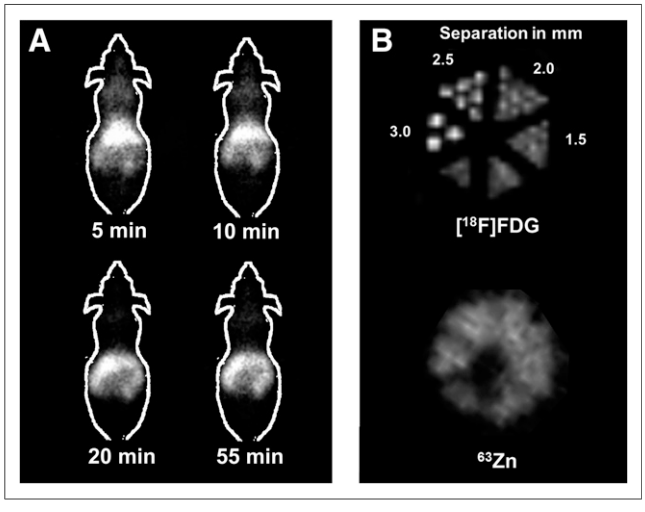

FIGURE 4. Small-animal PET images of normal mouse (A) after intravenous administration of ^{63}Zn-zinc citrate, and microresolution phantom (B) scanned with solutions of either ^{63}Zn or ^{18}F. Distance between filled capillary tubes of each resolution group is shown in mm. ^{63}Zn was not capable to resolve capillary tubes to maximum distance of 3.0 mm, whereas ^{18}F allowed for resolution to 2–2.5 mm.

DISCUSSION

Potential applications for PET imaging of zinc dynamics in a broad spectrum of diseases (*1–10*) motivates the development of a practical method for producing ^{63}Zn. Of the 3 known positron-emitting zinc isotopes, ^{63}Zn has the most favorable properties for quantitative PET imaging in humans (Table 1), although its 38.5-m half-life will limit investigations to under 2–3 h. Nevertheless, this time frame is sufficient to determine initial biodistribution patterns of zinc after intravenous injection and evaluation of fast to moderate tissue turnover times. The average positron energy of 0.992 MeV for ^{63}Zn is significantly higher than that of ^{18}F (0.25 MeV) but only slightly higher than ^{68}Ga (0.84 MeV) and ^{124}I (0.82 MeV). However, in comparison with ^{124}I, the high-energy γ emissions from ^{63}Zn are benign (Table 1). Thus, imaging spatial resolution is anticipated to be inferior to ^{18}F but on par with ^{68}Ga. Indeed, the phantom study in this work showed poorer spatial resolution in a small-animal PET resolution phantom relative to ^{18}F and noisier small-animal PET images than typically seen with ^{18}F-labeled radiotracers. These results are consistent with a detailed study of imaging of nonstandard PET radionuclides with small-animal PET (*15*).

As far as we are aware, this is the first reported method for producing radionuclidically pure ^{63}Zn ion for use as a PET imaging probe. An earlier study by Guerra-Goméz et al. (*12*) produced ^{63}Zn and small levels of ^{65}Zn ($T_{1/2}$, 244 d) contaminant after proton irradiation of natural copper foils. Because natural copper comprises 69.2% ^{63}Cu and 30.8% ^{65}Cu, enriched ^{63}Cu is modestly expensive and readily available as a starting material for solution targetry. We are not aware of a commercial source of isotopically enriched ^{63}Cu foil, but it could be electroplated onto a solid target mounting surface. Even so, our method would be more practical because it eliminates the need for acid dissolution of the solid target before isotope separation. The yields of ^{63}Zn-zinc citrate in our study (1–1.5 GBq) are sufficient to perform several human studies with the same batch (assuming multiple PET scanners are available simultaneously). Production yields can be augmented by increasing the ^{63}Cu-copper nitrate concentration in the target solution or increasing irradiation time. We are also working on further improvement of the target design to enhance heat transfer that we anticipate will support higher beam currents.

The final chemical form of ^{63}Zn in our method is zinc citrate, determined by the final elution of the carboxymethyl cartridge with commercially available isotonic sodium citrate solution. ^{63}Zn can also be eluted from the carboxymethyl cartridge using an isotonic histidine chloride solution (data not shown), but the elution efficiency is reduced. An advantage of using an isotonic 4% sodium citrate solution is that a USP-grade solution is commercially available for compliance with cGMP. We would assume that after entering the bloodstream, zinc would equilibrate among several potential binding agents, including serum albumin (*16*). Although albumin binds zinc with high affinity, the binding is characterized as exchangeable (*17*). Animal studies with ^{65}Zn have shown rapid exchange of the blood and tissue compartments (*18–20*). The QC HPLC method includes measurement of zinc, iron, copper, and nickel ions in the product solution. On the basis of available literature values of LD_{50} (lethal dose 50: dose at which 50% of animals are killed) for intravenous administration in animals, we have placed the maximum

acceptable limits of zinc, iron, copper, and nickel to be 0.026, 4.06, 1.03, and 25.8 g/L, respectively. The measured levels were well under 1% of these limits for all the metals.

The initial evaluation of ^{63}Zn-zinc citrate biodistribution in normal mice agrees with previous results with ^{65}Zn in rats (*19*). Zinc is essential for the normal processing, storage, secretion, and action of insulin in pancreatic β cells (*21*). The site of highest uptake of intravenously administered radiozinc is the pancreas, in which 2 Zn^{+2} ions coordinate 6 molecules of insulin within the storage vesicles of β cells (*21*). It is anticipated that ^{63}Zn PET may play an important role for the noninvasive assessment of zinc turnover in the pancreas in metabolic diseases, including metabolic syndrome, obesity, and diabetes. The distribution into the upper intestine at 60 min is likely due to pancreatic secretion of ^{63}Zn into the upper gut.

Liver uptake is also prominent because the liver is a highly metabolic organ that requires high levels of zinc associated with metabolic enzymes. As previously noted in other cancer types (*4–6*), hepatocellular carcinoma tumors consistently show marked decreases in zinc concentration, compared with normal liver (*22*), and thus zinc may serve as a biomarker for the early identification of malignancy. Other potential applications in the liver include monitoring of changes in liver zinc homeostasis in chronic active hepatitis and cirrhosis (*23*).

Finally, murine brain uptake of ^{63}Zn was moderately low but significant. Zinc is an important cofactor in neurotransmission in γ-aminobutyric acid– (*24*), glutamate- (*25*), and glycine-mediated (*26*) processes. Kanayama et al. (*27*) showed that ^{65}Zn uptake in rat brain at 30 min was severalfold higher than any of the other metal ions (beryllium, scandium, vanadium, chromium, manganese, iron, cobalt, arsenic, selenium, rubidium, strontium, yttrium, zirconium, technetium, and ruthenium) after administration as inorganic salts, demonstrating the robust transport of zinc across the blood–brain barrier. Interestingly, the same group showed markedly higher uptake of radioactive tracers of zinc, manganese, and rubidium in intracerebral C6 glioma tumors (*28*). In addition to potential ^{63}Zn PET imaging applications in neurology and neurooncology, we anticipate imaging applications in AD and Huntington disease. In these neurodegenerative diseases, a clear association has been made for zinc and copper metal ions in amyloid-β plaque formation and stabilization (*7,8*). Amyloid-β protein is reversibly precipitated by zinc and copper and coordinates these metals in plaques (*29*). Intracerebral zinc levels are highly abnormal in AD: postmortem analysis of brain samples in patients with AD showed that cortical zinc (but not copper) levels correlate with cognitive impairment (*30*). Metal chelator therapy directed at altering intracerebral zinc distribution is in active clinical investigation in AD (*8*), whereas zinc sulfate has been proposed as a therapy in Huntington disease (*31*). ^{63}Zn PET represents a new tool to begin to evaluate zinc transport in these various disease states and the effects of zinc-related therapies. Although the 38.5-min half-life of ^{63}Zn will limit measurements of slower (>2 h) intracellular zinc turnover times, it is anticipated that dynamic PET imaging data may provide quantitative assessments of transport and more rapid turnover processes.

CONCLUSION

A production method has been developed for the first time, to our knowledge, for radionuclidically pure ^{63}Zn based on solution target methods. The radiopharmaceutical preparation has been successfully tested according to standard cGMP QC tests. Uncorrected yields (at the end of the 30-min process) of 1.07 ± 0.22 GBq were obtained using a 1.23 M ^{63}Cu nitrate solution and proton irradiation at 20 μA for 60 min. If greater quantities of ^{63}Zn are needed, production levels can be readily increased by increasing the ^{63}Cu nitrate concentration or increasing irradiation time. Specific activity is sufficient not to significantly increase zinc levels in the blood in animal and human studies. A practical and efficient method of production of ^{63}Zn-zinc citrate has been developed that will enable PET imaging studies of zinc biodisposition and kinetics in animal and human studies.

DISCLOSURE

The costs of publication of this article were defrayed in part by the payment of page charges. Therefore, and solely to indicate this fact, this article is hereby marked "advertisement" in accordance with 18 USC section 1734. This work was supported by DOE (TRD/APB) DE-SC0008947. No other potential conflict of interest relevant to this article was reported.

ACKNOWLEDGMENTS

We thank Ray Steichen and Teresa Decklever at Mayo Clinic for their helpful assistance.

REFERENCES

1. Frassinetti S, Bronzetti G, Caltavuturo L, Cini M, Croce CD. The role of zinc in life: a review. *J Environ Pathol Toxicol Oncol.* 2006;25:597–610.
2. Penny ME. Zinc supplementation in public health. *Ann Nutr Metab.* 2013;62 (suppl 1):31–42.
3. Miao X, Sun W, Fu Y, Miao L, Cai L. Zinc homeostasis in the metabolic syndrome and diabetes. *Front Med.* 2013;7:31–52.
4. Costello LC, Levy BA, Desouki MM, et al. Decreased zinc and downregulation of ZIP3 zinc uptake transporter in the development of pancreatic adenocarcinoma. *Cancer Biol Ther.* 2011;12:297–303.
5. Kolenko V, Teper E, Kutikov A, Uzzo R. Zinc and zinc transporters in prostate carcinogenesis. *Nat Rev Urol.* 2013;10:219–226.
6. Alam S, Kelleher SL. Cellular mechanisms of zinc dysregulation: a perspective on zinc homeostasis as an etiological factor in the development and progression of breast cancer. *Nutrients.* 2012;4:875–903.
7. Craddock TJ, Tuszynski JA, Chopra D, et al. The zinc dyshomeostasis hypothesis of Alzheimer's disease. *PLoS ONE.* 2012;7:e33552.
8. Lannfelt L, Blennow K, Zetterberg H, et al. Safety, efficacy, and biomarker findings of PBT2 in targeting Abeta as a modifying therapy for Alzheimer's disease: a phase IIa, double-blind, randomised, placebo-controlled trial. *Lancet Neurol.* 2008;7:779–786.
9. Fujibayashi Y, Saji H, Kawai K, et al. A radiopharmaceutical for pancreatic exocrine functional diagnosis: ^{62}Zn-EDDA metabolism in pancreas. *Int J Nucl Med Biol.* 1986;12:447–451.
10. Takeda A. Movement of zinc and its functional significance in the brain. *Brain Res Brain Res Rev.* 2000;34:137–148.
11. Lyster DM, Noujaim AA. The unit dose preparation of ^{63}Zn-EDTA for use in nuclear medicine. *Int J Nucl Med Biol.* 1974;1:220–223.
12. Guerra-Gomez FLG, Takada Y, Hosoi R, et al. Production and purification of the positron emitter zinc-63. *J Labelled Compd Radiopharm.* 2012;55: 5–9.
13. Pandey MK, Engelbrecht HP, Byrne JP, Packard AB, Degrado TR. Production of ^{89}Zr via the ^{89}Y(*p,n*)^{89}Zr reaction in aqueous solution: effect of solution composition on in-target chemistry. *Nucl Med Biol.* 2014;41:309–316.
14. Pandey MK, Byrne JF, Jiang H. Packard AB, DeGrado TR. Cyclotron production of ^{68}Ga via the ^{68}Zn(*p,n*) ^{68}Ga reaction in aqueous solution. *Am J Nucl Med Mol Imaging.* 2014;4:303–310.
15. Liu X, Laforest R. Quantitative small animal PET imaging with nonconventional nuclides. *Nucl Med Biol.* 2009;36:551–559.
16. Blindauer CA, Harvey I, Bunyan KE, et al. Structure, properties, and engineering of the major zinc binding site on human albumin. *J Biol Chem.* 2009;284:23116–23124.

17. Lu J, Stewart AJ, Sadler PJ, Pinheiro TJ, Blindauer CA. Albumin as a zinc carrier: properties of its high-affinity zinc-binding site. *Biochem Soc Trans.* 2008;36:1317–1321.
18. Tibaduiza EC, Bobilya DJ. Zinc transport across an endothelium includes vesicular cotransport with albumin. *J Cell Physiol.* 1996;167:539–547.
19. Buxani-Rice S, Ueda F, Bradbury MW. Transport of zinc-65 at the blood-brain barrier during short cerebrovascular perfusion in the rat: its enhancement by histidine. *J Neurochem.* 1994;62:665–672.
20. Pullen RG, Franklin PA, Hall GH. ^{65}Zinc uptake from blood into brain and other tissues in the rat. *Neurochem Res.* 1990;15:1003–1008.
21. Li YV. Zinc and insulin in pancreatic beta-cells. *Endocrine.* 2014;45:178–189.
22. Costello LC, Franklin RB. The status of zinc in the development of hepatocellular cancer: an important, but neglected, clinically established relationship. *Cancer Biol Ther.* 2014;15:353–360.
23. Gür G, Bayraktar Y, Ozer D, Ozdogan M, Kayhan B. Determination of hepatic zinc content in chronic liver disease due to hepatitis B virus. *Hepatogastroenterology.* 1998;45:472–476.
24. Cohen-Kfir E, Lee W, Eskandari S, Nelson N. Zinc inhibition of gamma-aminobutyric acid transporter 4 (GAT4) reveals a link between excitatory and inhibitory neurotransmission. *Proc Natl Acad Sci USA.* 2005;102:6154–6159.
25. Nutini M, Frazzini V, Marini C, Spalloni A, Sensi SL, Longone P. Zinc pretreatment enhances NMDAR-mediated excitotoxicity in cultured cortical neurons from SOD1(G93A) mouse, a model of amyotrophic lateral sclerosis. *Neuropharmacology.* 2011;60:1200–1208.
26. Laube B. Potentiation of inhibitory glycinergic neurotransmission by Zn2+: a synergistic interplay between presynaptic P2X2 and postsynaptic glycine receptors. *Eur J Neurosci.* 2002;16:1025–1036.
27. Kanayama Y, Tsuji T, Enomoto S, Amano R. Multitracer screening: brain delivery of trace elements by eight different administration methods. *Biometals.* 2005;18:553–565.
28. Tamano H, Enomoto S, Oku N, Takeda A. Preferential uptake of zinc, manganese, and rubidium in rat brain tumor. *Nucl Med Biol.* 2002;29:505–508.
29. Adlard PA, Bush AI. Metals and Alzheimer's disease. *J Alzheimers Dis.* 2006;10:145–163.
30. Religa D, Strozyk D, Cherny RA, et al. Elevated cortical zinc in Alzheimer disease. *Neurology.* 2006;67:69–75.
31. Wu CL. Zinc sulfate could be a potential agent for the treatment of. Huntington's disease through activating central TrkB signaling. *CNS Spectr.* 2010;15:56–57.